Journal of Electroceramics, 13, 567–571, 2004

Microstructure of X7R Type Base-Metal-Electroded $BaTiO_3$ Capacitor Materials Co-Doped with MgO/Y_2O_3 Additives

CHENG-SAO CHEN,[1,2] CHEN-CHIA CHOU[1] & I-NAN LIN[3,*]

[1]*Department of Mechanical Engineering, National Taiwan University of Science and Technology, Taipei 106*
[2]*Department of Mechanical Engineering, Hwa-Hsia College of Technology and Commerce, Chungho 235*
[3]*Department of Physics, Tamkang University, Tamsui 251, Taiwan, Republic of China*

Submitted March 3, 2003; Revised March 10, 2004; Accepted March 17, 2004

Abstract. Detailed microstructure of MgO/Y_2O_3 co-doped $BaTiO_3$ materials were examined using transmission electron microscopy (TEM). For the 1250°C-sintered $BaTiO_3$ samples possessing flat K-T characteristics, which meet the X7R specification, the granular structure is complicated. Most of the grains are very small (∼150 nm) and are highly strained. The small grains contain large proportion of Y_2O_3 species and are paraelectric, whereas the large grains contain Y_2O_3 species unevenly distributed and are of core-shell structure. In contrast, for the 1300°C-sintered $BaTiO_3$ samples, which have K-T properties slightly off the X7R specification, the grains grew larger to around 300 nm. The core-shell structured grains are seldom observed. Apparently, it is the existence of such a non-equilibrium core-shell microstructure, which renders the dielectric properties of the $BaTiO_3$ materials extremely sensitive to the processing parameters.

Keywords: transmission electron microscopy, base-metal-electroded capacitor, $BaTiO_3$, X7R

1. Introduction

High performance and small sized multilayer ceramic capacitors (MLCC), which possess high reliability and compatible with surface mounting technology, have great potential for industrial applications [1]. Technology for MLCC mainly involves the co-firing of dielectrics and electrode materials (Ag/Pd alloy). However, utilization of large Pd content electrode materials increases the manufacturing cost tremendously. The development of inexpensive electrode materials such as base metals (Cu and Ni) is thus urgently needed for reducing the production cost for MLCC [2, 3]. The base-metal-electroded (BME) capacitors need to be fired under reducing atmosphere, since the Cu (or Ni) metal is subjective to oxidation during sintering in air. Many approaches were reported being able to successfully maintain high insulation resistance of the $BaTiO_3$ materials after sintering in reduced atmosphere [3–10].

*To whom all correspondence should be addressed. E-mail: inanlin@mail.tku.edu.tw

The most important dielectric characteristics of concern for MLCC capacitor materials is the capacitance variation ($\Delta C/C$) in operation temperature regime. For example, in X7R type MLCC materials, the $\Delta C/C$-value must be within $\pm 15\%$ in the temperature regime from –55° to 125°C. The key factor resulting in low temperature coefficient of dielectric properties is presumed to be the presence of the core-shell microstructure [11–14], which can be achieved by precisely controlling the doping species and concentration [15–17]. Previously, we have reported the effect of Yttrium oxide, Y_2O_3, and Magnesium oxide, MgO, additions on the dielectric properties of the $BaTiO_3$ materials [17]. The dielectric properties, especially the temperature dependence of capacitance variation, of the $BaTiO_3$ materials were improved markedly but the detailed mechanism is still not well understood.

In this paper, we examined the microstructure of these materials in detail using transmission electron microscopy (TEM) so as to explore the formation mechanism of the core-shell microstructures. We also correlated the materials' microstructure with their dielectric properties, based on these observations.

2. Experimental

In the synthesis of the core-shell structured materials, the commercial $BaTiO_3$ powders (0.2 μm) were mixed with the dopants [Y_2O_3 (1.5 mol%), MnO_2(0.4 mol%) and MgO (2 mol%)] and sintering aids [$(Ba_{0.6}Ca_{0.4})SiO_3$, 3 mol%]. The mixtures were pressed and then sintered at 1250–1300°C for 3 h in 10^{-10} torr Po_2 atmosphere, followed by re-oxidization at 1000°C for 2 h in 6.08×10^{-2} torr Po_2 atmosphere. The microstructures of the samples, which were polished and then chemically etched, were examined using scanning electron microscopy (SEM, Joel TSM-840 A). The Cu-paste was screen printed onto the sintered samples, followed by firing at 900°C for 10 min in 2.28×10^{-2} torr Po_2 atmosphere to serve as electrodes. The dielectric properties of the capacitor materials were measured from −55 to 150°C using HP 4278 capacitance meter. The detailed microstructure of the samples was examined using transmission electron microscopy (TEM, Joel 2000 FX II), whereas the composition distribution was measured using EDAX in TEM (Philips TECNAI F30).

3. Results and Discussion

To maintain the ΔC/C in a small value, the processing conditions need to be controlled in very narrow range even when the concentration of additives was stringently monitored. Figure 1(a) shows that the $BaTiO_3$ materials sintered at 1250°C(3 h) possess relatively flat dielectric constant-temperature (K-T) properties (open circles) such that the capacitance variation (ΔC/C) was maintained smaller than ±15% in between −55°C and +125°C temperature regime, viz. these materials meet X7R specification (Fig. 1(b), open circles). Sintering at higher temperature (1300°C, 3h) results in slight change in K-T behavior (Fig. 1(a), solid squares) such that the ΔC/C characteristics is off the X7R specification (Fig. 1(b), solid squares). Presumably, the high sintering temperature affects the dielectric behavior of the materials through the modification on their microstructure. However, the SEM microstructures for these samples are very similar to one another, which are illustrated as a typical SEM micrograph in Fig. 1(c). All of the materials contain very fine grains with uniform grain size distribution. To understand genuine mechanism altering the K-T properties of the

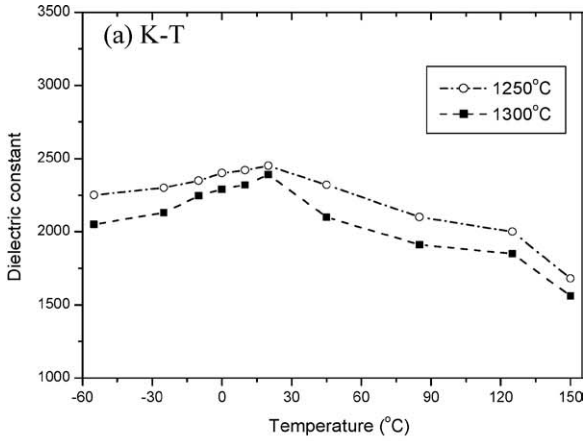

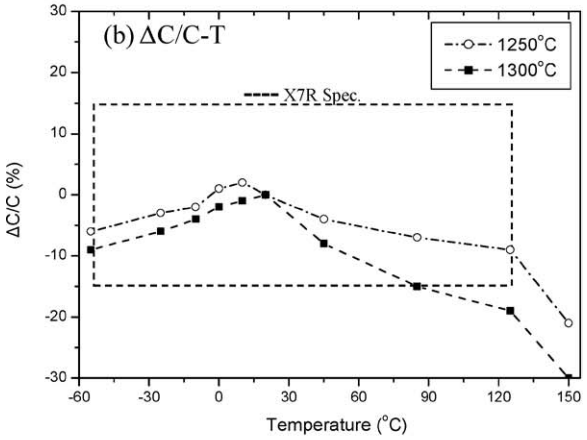

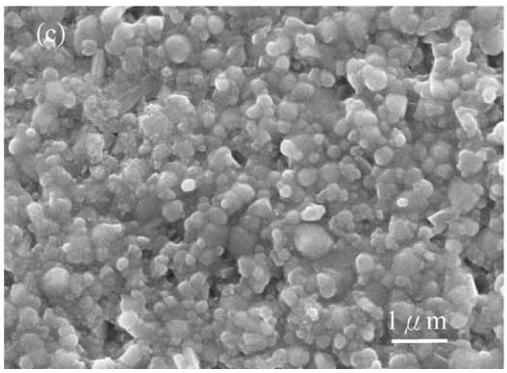

Fig. 1. (a) Dielectric constant-temperature, K-T, and (b) capacitance variation-temperature, ΔC/C properties of the 1250°C 1300°C–sintered $BaTiO_3$ materials; (c) typical SEM micrograph of these samples ($BaTiO_3$ materials contain 1.5 mol% Y_2O_3, 2 mol% MgO, 0.4 mol% MnO_2 as dopants and 3 mol% $(Ba_{0.6}Ca_{0.4})SiO_3$ as the sintering aid).

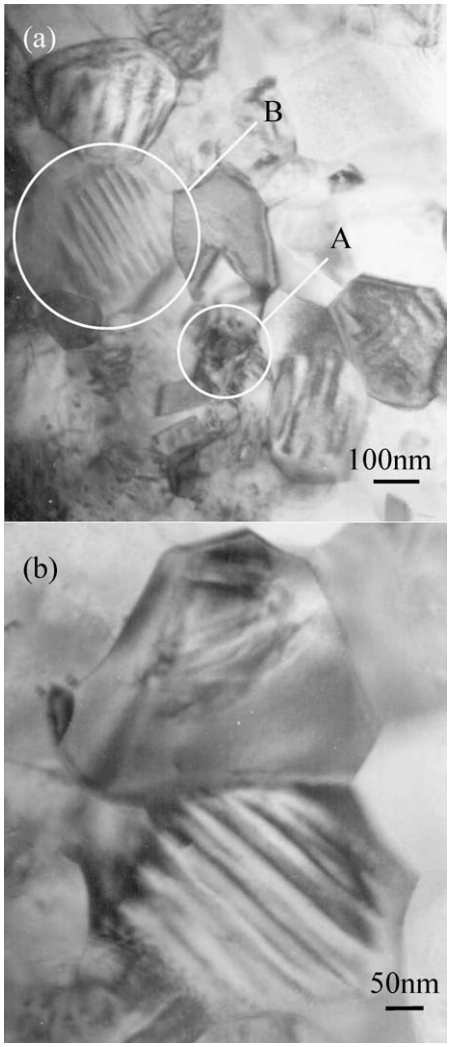

Fig. 2. (a) TEM microstructure of a 1250°C—sintered $BaTiO_3$ materials and (b) enlarged TEM micrograph of a core-shell structured grains ($BaTiO_3$ materials contain 1.5 mol% Y_2O_3, 2 mol% MgO, 0.4 mol% MnO_2 as dopants and 3 mol% $(Ba_{0.6}Ca_{0.4})SiO_3$ as the sintering aid).

$BaTiO_3$ materials, detailed microstructure examined by using transmission electron microscopy (TEM) is needed.

Figure 2 shows the typical microstructure of a 1250°C-sintered X7R type capacitor materials. The grains are very small, around 100–200 nm, and are very uniformly distributed. The smaller grains contain large proportion of strain contrast (grain A, Fig. 2(a)). Only when the grains grew to a larger size (∼200 nm), stripe patterns are observed (grain B, Fig. 2(a)). The stripe patterns are similar to the electric domains frequently observed in $BaTiO_3$ materials, indicating that this region is ferroelectric. Enlarged micrograph of grain B (Fig. 2(b)) indicates that there exists a shell surrounding the ferroelectric region, resulting in a core-shell microstructure. The grain boundaries are usually blurred. The shell region shows no feature at all even we tilted the samples in TEM, inferring that it is a paraelectric phase. Moreover, the shell is not uniformly surrounding the core region and their thickness varies among the grains.

In contrast, Fig. 3(a) shows that the general features of the microstructure 1300°C-sintered samples are the same as those of 1250°C-sintered ones, i.e., the grains are small and uniform, except that the average grain size of these materials is slightly larger (∼200–300 nm). Again, smaller grains are highly strained and larger grains contain domain structure, which are better illustrated as Fig. 3(a) and (b), respectively. The smaller grains are paraelectric and the larger grains are ferroelectric. Moreover, the proportion of ferroelectric grains is larger in the 1300°C-sintered materials than that in 1250°C-sintered specimens. Occasionally, the core-shell structured grains were observed for the large grains, in which the shell-to-core thickness ratio is much smaller (Fig. 3(c)). The grain boundaries are much clearly defined, indicating that the microstructure has been more completely developed. These results indicate that the core-shell structure is a non-equilibrium microstructure and is thus sensitive to the thermal history of the samples. Therefore, the dielectric constant-temperature (K-T) behavior for the Y_2O_3/MgO co-doped materials is highly process dependent.

For the purpose of understanding of the formation process for such a complicated microstructure, the compositional profile of a large core-shell structured grain and a small strained grain in 1250°C-sintered ones were examined using EDAX in TEM. Figure 4 shows the typical EDAX spectrum. The concentration of the core/shell (or center/boundary) regions was extracted from the respective EDAX spectra and was listed in Table 1. Table 1(a) indicates that, for the core-shell structured grains, the concentration of the main constituents, Ba and Ti, varies insignificantly over the region, whereas the Y-content in shell region is markedly larger than that in core region. The Mg-content in the two regions is not significantly different from each other. These results infer that Y_2O_3-addition alters the dielectric properties of the $BaTiO_3$ materials more pronouncedly than the MgO does. In contrast,

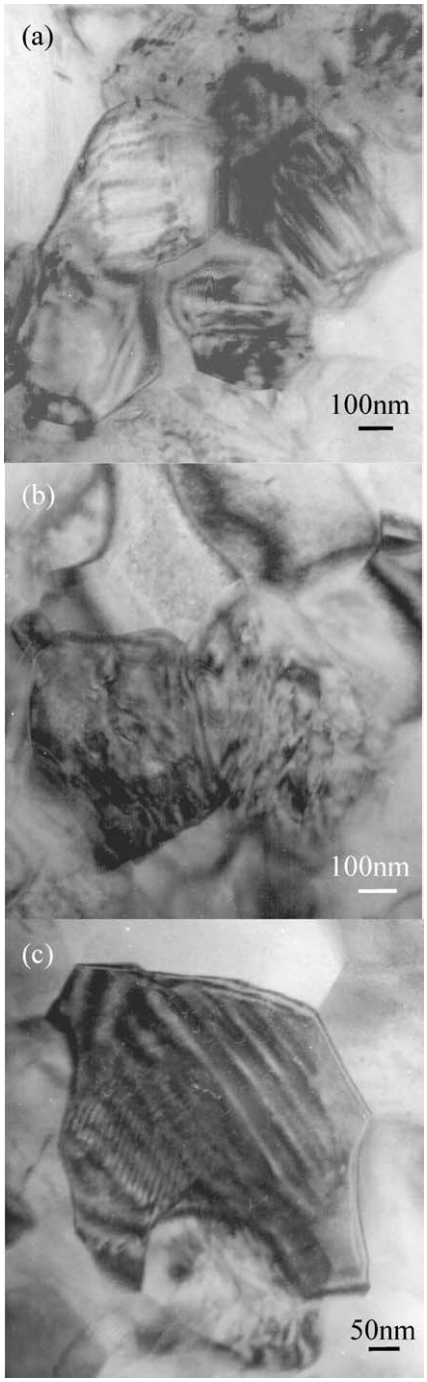

Fig. 3. (a) TEM microstructure of a 1300°C—sintered $BaTiO_3$ materials, (b) enlarged TEM micrograph of a strained paraelectric grains and (c) enlarged TEM micrograph of a core-shell structured ferroelectric grains ($BaTiO_3$ materials contain 1.5 mol% Y_2O_3, 2 mol% MgO, 0.4 mol% MnO_2 as dopants and 3 mol% $(Ba_{0.6}Ca_{0.4})SiO_3$ as the sintering aid).

Table 1. The composition of the (a) core-shell structured and (b) paraelectric $BaTiO_3$ grains analyzed from EDAX in TEM.[a]

	Ba	Ti	Y	Mg
(a) Core-shell structured grains				
Core region	1.55	9.11	0.38	0.39
Shell region	1.22	8.97	1.20	0.41
(b) Paraelectric grains				
Center region	1.55	9.45	1.00	0.39
Boundary region	1.67	9.82	0.92	0.36

a Composition in mol%.

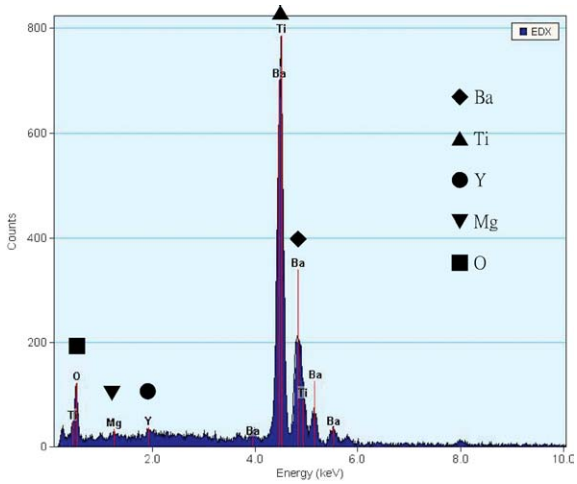

Fig. 4. Typical composition of the $BaTiO_3$ materials analyzed by EDAX in TEM.

Table 1(b) reveals that in the highly strained small grains, both the center and boundary regions contain the same high concentration of Y_2O_3 (or MgO) species. The Y_2O_3-content in these samples is pronouncedly larger than, whereas the MgO-content is not much different from, those in the core region of the core-shell grains. High Y_2O_3-content in these strained grains indicates that it is the large Y_2O_3-content incorporated in these grains, which induces large distortion on the perovskite lattices and suppressing the growth of grains.

4. Conclusion

Microstructures of core-shell structured $BaTiO_3$ materials were examined in detail by transmission electron microscopy (TEM) to correlate the microstructure

of these materials with their dielectric properties. The grains, which contain paraelectric shell surrounding the ferroelectric core, are frequently observed for 1250°C-sintered samples. The thickness of the shell was diminished as the grains grow to a larger size, whenever the samples were sintered at 1300°C. The variation of the core-shell microstructure of the samples with the thermal history of the materials explain very well the K-T properties being extremely sensitive with processing parameters for these materials.

Acknowledgments

Financial support from National Science Council, R. O. C. through the project no. NSC 91-2822-E-007-032 is gratefully acknowledged by the authors.

References

1. Y. Sakabe, T. Takagi, and K. Wakino, *J. Am. Ceram. Soc*., **69**, 103 (1986).
2. S. Sato, Y. Nakano, and A. Sato, *Jpn. J. Appl. Phys.*, **9B**, 6016 (1996).
3. H. Shizuno, S. Kusumi, and H. Saito, *Jpn. J. Appl. Phys.*, **9B**, 4380 (1993).
4. C.J. Peng and H.Y. Lu, *J. Am. Ceram. Soc.*, **71**, C44 (1988).
5. M. Drodenik, *J. Am. Ceram. Soc.*, **70**, 311 (1987).
6. H.M. Chan, M.P. Harmer, and D.M. Smyth, *J. Am. Ceram. Soc.*, **69,** 507 (1986).
7. M. Kahn, *J. Am. Ceram. Soc.*, **54**, 455 (1971).
8. S. Sumita, M. Ikeda, Y. Nakano, K. Nishiyama, and T. Nomura, *J. Am. Ceram. Soc.*, **74**, 2739 (1991).
9. I. Burn, *Ceram. Bulletin*, **57**, 600 (1978).
10. W.C. Yang, C.T. Hu, and I.N. Lin, *Ferroelectrics*, **270**, 1321 (2002).
11. N.M. Molokhia, M.A. Issa, and S.A. Nasser, *J. Am. Ceram. Soc.*, **67**, 289 (1984).
12. Y. Park and H.G. Kim, *J. Am. Ceram. Soc.*, **80**, 106 (1997).
13. D. Hennings and G. Rosenstein, *J. Am. Ceram. Soc.*, **67,** 249 (1984).
14. H. Kishi, Y. Mizuno, and H. Chazono, *Jpn, J. Appl. Phys.*, **42**, 1 (2003).
15. H. Saito, H. Chazono, H. Kishi, and N. Yamaoka, *Jpn. J. Appl. Phys.*, **9B**, 2307 (1991).
16. Y. Mizuno, Y. Okino, N. Kohzu, H. Chazono, and H. Kishi, *Jpn. J. Appl. Phys*., **9B**, 5227 (1998).
17. W.C. Yang, C.T. Hu, and I.N. Lin, *J. Euro. Ceram. Soc.*, **24**, 1479 (2003).